One-Step Synthesis and Optical Properties of Benzoate- and Biphenolate-Capped ZrO_2 Nanoparticles

Xue Bai, Andrea Pucci, Vania T. Freitas, Rute A. S. Ferreira, and Nicola Pinna**

A simple one-pot approach based on the "benzyl alcohol route" is used for the preparation of benzoate- and biphenolate-capped zirconia and, benzoate-capped Eu-doped zirconia nanoparticles. Powder X-ray diffraction studies and high- resolution transmission electron microscopy (HR-TEM) showed that the nanoparticles present high crystallinity and uniform particle sizes ranging from 3 to 4 nm. FT-IR and solid state NMR (SS-NMR) studies revealed that the nanoparticles are coated with a large amount of organic species when the reaction temperature is above 300 °C. It was found that the alcohol used as solvent is oxidized at the surface of the nanoparticles to the respective carboxylic acid which acts as a stabilizer, controlling the nanoparticles growth. The optical properties of these hybrid nanoparticles were studied by room and low (12K) temperature photoluminescence spectroscopy, time-resolved spectroscopy and absolute emission quantum yield. The as-synthesized benzoate- and biphenolate-capped nanoparticles exhibit interesting emission properties in the UV and blue spectral regions together with values of emission quantum yields much higher than those reported for zirconia nanoparticles of similar size. The photoluminescent properties were attributed to a cooperative effect of the capping ligands and the defects associated to the ZrO_2 nanoparticles. Due to the overlapping of the various emission components involved (i.e., the emission of europium(III) intra-$4f^6$ transitions, defects in the zirconia and capping ligands) a tunable emission color ranging from purplish-pink to greenish-blue could be obtained for the europium-doped zirconia nanoparticles by simply selecting different excitation wavelengths.

1. Introduction

Zirconia (ZrO_2) is an important metal oxide ceramic material that has been intensively studied for both scientific aspects and technological applications.[1–10] Due to its wide band gap,[11,12] high refractive index[13] and low toxicity[14] ZrO_2 nanoparticles have been exploited in various fields, such as high temperature solid oxide fuel cells,[1–3] catalysis,[4–6] solar cells,[7,8] optical gratings[9,13] and sensors.[10] Recently, much interest was focused on the luminescent properties of pure as well as doped ZrO_2 nanoparticles.[15–20] ZrO_2 is highly transparent in both UV and visible ranges, and its optical absorption occurs below 250 nm due to its wide band gap above 5 eV.[12] For white LEDs applications, efficient phosphors that can convert low energy UV radiation into light are sought after.[21–23] The main challenge is to develop stable, efficient, and environmental friendly nanophosphors that can be excited between 340 and 400 nm. Some methods have been developed to improve the luminescence properties of ZrO_2 nanoparticles by inducing a red-shift and broaden the excitation band.[24–26] Among these studies a common approach is based on post-synthesis functionalization of the metal oxide nanoparticles with organic molecules, forming organic-inorganic nanocomposite materials with improved luminescence properties.[24,27,28] Nevertheless, these processes are generally complex, not very effective and difficult to scale up.[27]

In the past few years, surfactant-free nonaqueous sol-gel approaches have been developed for the synthesis of various metal oxide nanoparticles and organic-inorganic materials through simple routes.[9,13,29] In this paper, we present a one-step nonaqueous synthesis of benzoate- and biphenolate-capped ZrO_2 nanoparticles. The solvent used for the synthesis (i.e. benzyl alcohol and biphenyl methanol) is oxidized to the respective carboxylate species on the surface of the freshly formed inorganic network, controlling

Dr. X. Bai, Dr. A. Pucci, Prof. N. Pinna
Department of Chemistry, CICECO
University of Aveiro
3810-193 Aveiro, Portugal
E-mail: pinna@ua.pt
V. T. Freitas, Dr. R. A. S. Ferreira
Department of Physics, CICECO
University of Aveiro
3810-193 Aveiro, Portugal
E-mail: rferreira@ua.pt

DOI: 10.1002/adfm.201200759

Prof. N. Pinna
World Class University (WCU) program of Chemical Convergence for Energy & Environment (C2E2)
School of Chemical and Biological Engineering
College of Engineering
Seoul National University (SNU)
Seoul 151-744, Korea
E-mail: pinna@snu.ac.kr

Table 1. The table provides the inorganic phase, carbon content, reaction temperature, nanoparticle sizes and organic species at the surface of the nanoparticle for the different samples studied.

Inorganic Material	Carbon Content [weight%][a)]	Reaction Temperature [°C]	Particle Size [nm][b)]	Organic Species
ZrO_2	3.3	250	3.8	Benzoate
ZrO_2	8.96	300	4.1	Benzoate
ZrO_2	17.59	300	3.2	Biphenolate
ZrO_2	8.13	300	4.1	Undecanoate+ Benzoate
ZrO_2:Eu	9.54	300	3.3	Benzoate

[a)]Deduced from CHN analysis; [b)]Crystallite size estimated from XRD patterns using the Scherrer equation and considering the diffraction peak at $2\theta = 50°$ (i.e., 220).

the nanoparticles growth and stabilizing them. The structure, composition, growth mechanism, and photoluminescence properties were studied. The impact of benzoate and biphenolate ligands on the optical properties of the nanoparticles is discussed in detail. Moreover, time-resolved spectroscopy points out, beside the organic ligands contribution, that the emission is also governed by a defect-related component displaying a donor-acceptor (D-A) recombination mechanism. The point defects, particularly those related to oxygen vacancies, were thus considered responsible for the luminescence properties. Further understandings on the origin of the luminescence were obtained by exchanging the organic moieties with an aliphatic counterpart (i.e. undecanoic acid) and by doping the zirconia matrix with europium(III) ions.

2. Result and Discussion

2.1. Structure and Morphology Characterization

The synthesis of zirconia nanoparticles relies on the solvothermal reaction of the metal oxide precursor (i.e., zirconium isopropoxide isopropanol complex) with an organic solvent (i.e., benzyl alcohol), which is a versatile reaction system for the nonaqueous preparation of oxide nanoparticles as it was previously reported.[29a,b] Compared to previous reports[9,13,29e,f] the zirconia nanoparticles studied in this work were synthesized at higher temperature (250 and 300 °C compared to 210–230 °C). As a matter of fact, a higher reaction temperature leads to the formation of a larger amount of organic molecules absorbed at the surface of the nanoparticles (see below). In addition to benzyl alcohol, the synthesis was also carried out in biphenyl-4-methanol, likewise under the same conditions (cf. **Table 1**). Finally, to best assess the optical properties, zirconia particles synthesized in benzyl alcohol at 300 °C were, in some cases, doped with 2% of europium(III) or post-functionalized with undecanoic acid.

In order to evaluate the size, morphology and, crystallinity, the samples were characterized by powder X-ray diffraction (XRD) and transmission electron microscopy (TEM). Their XRD patterns (**Figure 1**) present broad peaks due to the nanometric size of the crystallites. The position as well as the relative intensity of the peaks match well with the one of the cubic ($Fm\bar{3}m$) or tetragonal ($P4_2/nmc$) crystal structures of

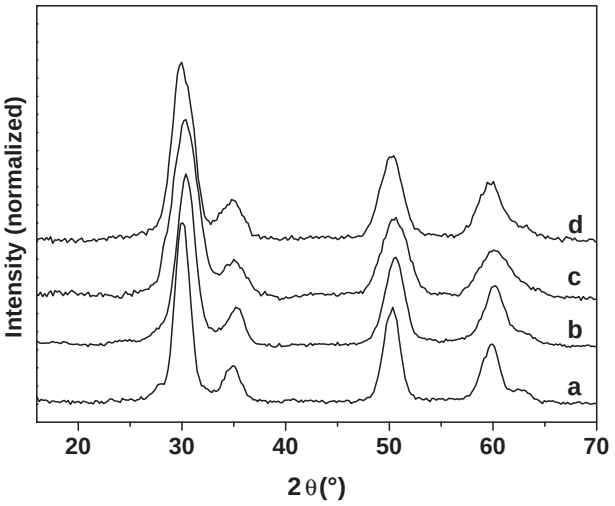

Figure 1. XRD patterns of ZrO_2 nanopowders prepared under different synthesis conditions: a) synthesized in benzyl alcohol at 300 °C for 36 h; (b) synthesized in benzyl alcohol at 250 °C for 36 h; c) synthesized in biphenyl-4-methanol at 300 °C for 36 h; d) Eu^{3+}-doped ZrO_2 synthesized in benzyl alcohol at 300 °C for 36 h.

zirconia.[29j] Using the Scherrer equation the crystallite size was evaluated to be 4.1, 3.8, and 3.2 nm for the samples synthesized at 300 and 250 °C in benzyl alcohol and in biphenyl-4-methanol, respectively. Noteworthy, as it will be discussed below, the crystallite size corresponds also to the particle size and does not strongly depend on the reaction temperature and solvent used (cf. Table 1). Moreover, as already observed in previous studies, the nanoparticle and crystallite sizes, estimated from XRD and TEM, slightly decrease upon doping with transition metals and rare earth ions.[9,29g,j] The replacement of the benzyl alcohol with biphenyl-4-methanol has a similar effect on the particle size (Table 1).

Figure 2 presents the TEM images of representative areas of the zirconia nanoparticles synthesized in benzyl alcohol at 250 °C (a) and in biphenyl-4-methanol at 300 °C (d). The nanoparticles are generally homogeneous in size and shape. The sizes extracted from TEM are in good agreement with the values derived from XRD measurements, indicating the single crystalline nature of the nanoparticles. This is also supported by HR-TEM measurements (Figure 2b) showing an isolated 3 nm ZrO_2 nanoparticle displaying well defined lattice fringes. The

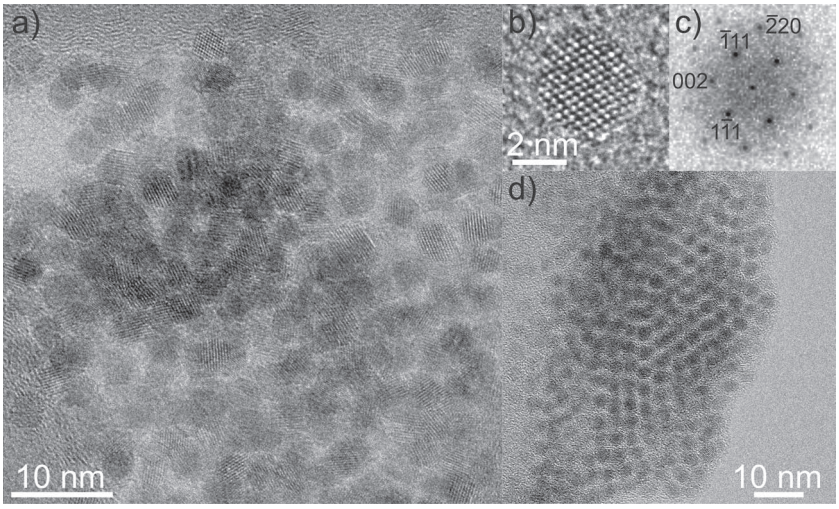

Figure 2. TEM (a) and HR-TEM (b) images of ZrO_2 nanoparticles synthesized in benzyl alcohol at 250 °C. (c) Power spectrum of the nanocrystal in (b) demonstrating that the ZrO_2 particle is oriented along the [110] axis. (d) TEM of ZrO_2 nanoparticles synthesized in biphenyl-4-methanol at 300 °C.

distances and the angles between reflections extracted from the power spectrum (Figure 2c) match well those of the cubic ZrO_2 structure along the [110] zone axis.

From the TEM images it seems that the nanoparticles synthesized at high temperature and especially those synthesized in biphenyl-4-methanol instead of benzyl alcohol present a large amount of carbon species adsorbed at their surface. For example, Figure 2d shows that the nanoparticles are enclosed in an amorphous carbon matrix. This is also proven by the fact that under the electron beam a contamination layer grows rather rapidly. This is generally not observed for inorganic nanoparticles free of carbon-containing molecules such as surfactants. Table 1 gives the carbon content evaluated by CHN elemental analysis, which is around threefold larger when the reaction temperature increases from 250 to 300 °C. A twofold increase is also recorded when benzyl alcohol is replaced by biphenyl-4-methanol, reaching carbon contents above 17% in weight.

The normalized FT-IR spectra of the various samples are shown in **Figure 3**. Intense infrared vibrations of the organic species absorbed onto ZrO_2 nanoparticles are clearly visible. The curve (a) presents the FT-IR spectrum of the sample synthesized in benzyl alcohol at 300 °C. The peaks appearing at 1598, 1496, and 1450 cm^{-1} are associated to the C=C stretching modes of the phenyl rings.[30] The strong absorptions at 1542 and 1434 cm^{-1} correspond to the asymmetric (υ_{as}) and symmetric (υ_s) stretching vibration of carboxylate ($-COO^-$) groups,[30–32] denoting that benzoate species are absorbed onto ZrO_2 nanoparticles. These data were further confirmed by solid state NMR (SS-NMR) experiments (see below). The coordination mode of the $-COO^-$ group linked to the zirconium ions can be assessed by the difference of frequency between the two carboxylate stretching vibrations ($\Delta = \upsilon_{as} - \upsilon_s$). The relative difference in Figure 3a accounts to $\Delta = 108$ cm^{-1}, indicating chelating bidentate coordinated carboxylate species.[30,33] It is interesting to note that the two shoulders appearing at around 1631 and 1366 cm^{-1} can be associated to the C=O and C-O stretching vibration of monodentate carboxylates.[30] This result indicates that there are two types of coordination, although the chelating bidentate is favored as the higher intensity of the bands suggests. Figure 3b shows the FT-IR spectrum of the sample synthesized at 250 °C. The similar value of $\Delta = 112$ cm^{-1} also points to a chelating bidentate coordination. Moreover, the intensity of the vibrations from the carboxylate group in monodentate coordination increases compared to the chelating coordination while the synthesis temperature decreases. In the case of biphenyl-4-methanol (curve c), two bands at 1608 and 1573 cm^{-1} appear while the intensity of the band at 1450 cm^{-1} decreases caused by the phenyl moiety being replaced by biphenyl one. The asymmetric and symmetric stretching vibrations of the carboxylate species are visible at 1535 and 1442 cm^{-1}, respectively, indicating that biphenolate species are coordinated to the surface of ZrO_2 nanoparticles with a chelating character stronger than the one of monoaromatic species ($\Delta = 93$ cm^{-1}). The two shoulders around 1631 and 1366 cm^{-1} are not present in this sample denoting the absence of monodentate coordination.

Curve (d) shows the FT-IR spectrum of the sample modified with undecanoic acid. A new broad absorption peak was observed at 1467 cm^{-1}, which is the sum of three contributions: i) the scissoring stretching of $-CH_2-$ group in undecanoic acid. ii) The symmetric stretching of the carboxylate belonging to the aliphatic chain. The difference between this peak and the asymmetric one ($\Delta = 86$ cm^{-1}) suggests a strong chelating character. iii) The stretch modes (1450 cm^{-1}) of the phenyl rings still present on the surface. Other peaks associated with benzoate are also visible, such as the vibration modes of the phenyl rings (1598 and 1496 cm^{-1}) and the symmetric stretching of the carboxylic moiety (1426 cm^{-1}). By comparing the intensity of these

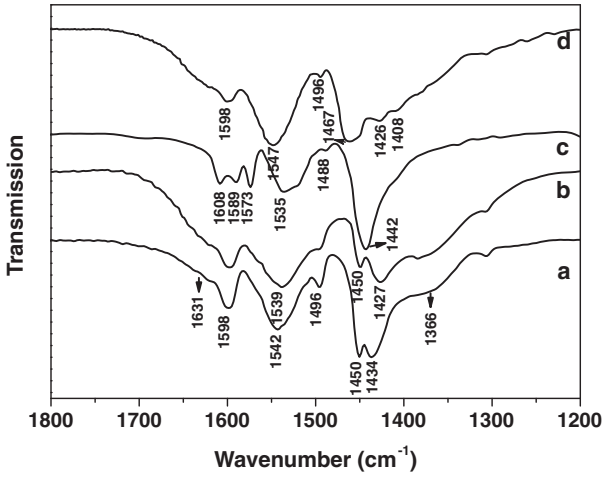

Figure 3. FT-IR absorption spectra of ZrO_2 nanoparticles: (a) synthesized in benzyl alcohol at 300 °C; (b) synthesized in benzyl alcohol at 250 °C; (c) synthesized in biphenyl-4-methanol at 300 °C; (d) the sample synthesized in benzyl alcohol at 300 °C modified with undecanoic acid.

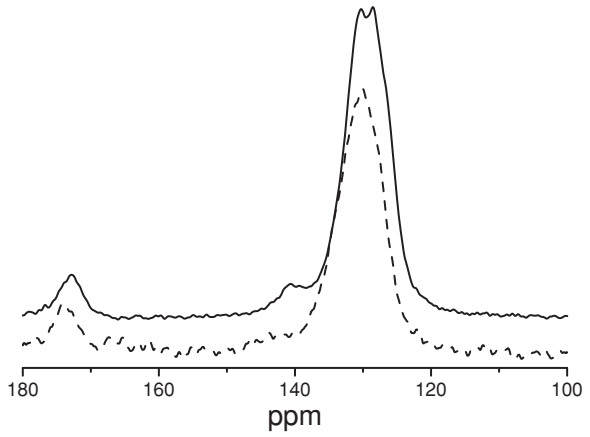

Figure 4. ^{13}C Solid State NMR spectra of ZrO_2 nanoparticles synthesized at 230 (dashed line) and 300 °C (full line).

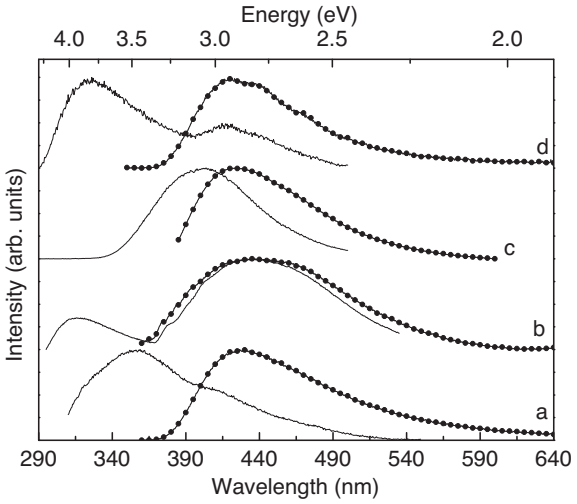

Figure 5. Room temperature emission spectra of the ZrO_2 nanoparticles (a) synthesized in benzyl alcohol at 250 °C, (c) in biphenyl methanol and (d) modified with undecanoic acid. (b) Emission spectra acquired at 12 K for the sample synthesized in benzyl alcohol at 250 °C. Excited at 280 nm (solid lines) and 335–360 nm (lines with circles).

peaks with those of the pristine sample, an evident decrease of the intensity is observed, indicating that most of the benzoate species were replaced by undecanoic acid molecules during the functionalization process. This will be assuredly confirmed by the luminescence results (see below). It is worth to note that the absence of an absorption at ~1710 cm^{-1}, assigned to the C=O bond in polar group of undecanoic acid, indicates that the undecanoic acid is present only in its deprotonated form proving the complete adsorption onto the zirconia surface.[33]

The ^{13}C SS-NMR spectra of pure zirconia samples (**Figure 4**) show interesting feature only between 100 and 180 ppm. They display a broad band between 121 and 137 ppm, a small peak centered at 140 ppm and a peak at lower field centered at 173 ppm. In general, the spectrum recorded on the sample synthesized at higher temperature (full line), carrying a larger amount of organics, is better resolved. Considering the kind of organics playing a role in the reaction (benzyl alcohol as solvent and isopropyl moieties of the zirconium precursor) the patterns can be easily traced back to benzoate species matching well potassium benzoate salt reported in literature.

From this study, it can be concluded that at reaction temperatures ranging from 230 to 300 °C the alcohol used as solvent can be oxidized to the respective carboxylate species coordinating onto the surface of the freshly formed zirconia nanoparticles. The *in situ* produced organic ligands permit to control the nanoparticles growth resulting in the formation of almost monodisperse nanoparticles. Although the formation mechanism of zirconium oxide is based on the ether elimination condensation reaction between metal alkoxides as it has been described previously,[29a] it is also clear that the high temperatures used in this work promote the formation of carboxylates probably following the reaction mechanism found in the case of rare earth oxide hybrid materials synthesized in benzyl alcohol.[29c,d] Interestingly, only traces of a derivative of benzoic acid (benzylbenzoate) were found in the reaction mother liquor after nanoparticles formation (not shown), suggesting that benzoate species are formed at the surface of the nanoparticles, stay absorbed and control their growth. These carboxylate ligands not only play an important role in controlling the nanoparticle size, but also have a strong influence on the luminescence properties.

2.2. Optical Characterization

Under UV excitation, the as-synthesized samples exhibit wide emission bands spanning from the UV to the visible spectral regions. **Figure 5** presents the emission spectra acquired at 12 and at 300 K for the sample synthesized in benzyl alcohol at 250 °C excited at distinct wavelengths. For excitation wavelengths between 300 and 375 nm, the low-temperature emission spectra reveal the presence of a single broad (full width at half maximum, FWHM, ca. 120 nm) component peaking at ca. 440 nm (2.81 eV), ascribed to the excited states of the phenyl rings of the benzoate molecules.[29d] At lower excitation wavelengths (250–300 nm), one more component at *ca*. 320 nm (3.90 eV) appears, which may be related to the zirconia nanocrystals, as detailed below.

The low-temperature excitation paths of each emission component were selectively monitored at the respective maximum intensity peak position (**Figure 6**). The excitation spectrum monitored within the main emission component (440 nm) reveals the presence of three broad UV components at *ca*. 260, 290 and 340 nm (4.80, 4.28 and 3.60 eV, respectively); whereas monitoring the low-intensity emission component (320 nm), only the low-wavelength UV bands (peaking at 260 and 290 nm) could be detected, pointing out that the benzoate-related emission component is selectively excited within the range 350–400 nm.[29d] The low wavelength-region (240–290 nm), resembles the excitation spectrum previously reported for monodisperse tetragonal zirconia nanocrystals with similar size,[34] being ascribed to the presence of surface trap or defect states, involving extrinsic states as the emission energy displays a red-shift when compared to the one found for bulk zirconia.[12] The origin of the intrinsic photoluminescence in pure ZrO_2 nanoparticles is still an open discussion being often mentioned in the literature that the defect-related emission is due to the presence of oxygen vacancies or point

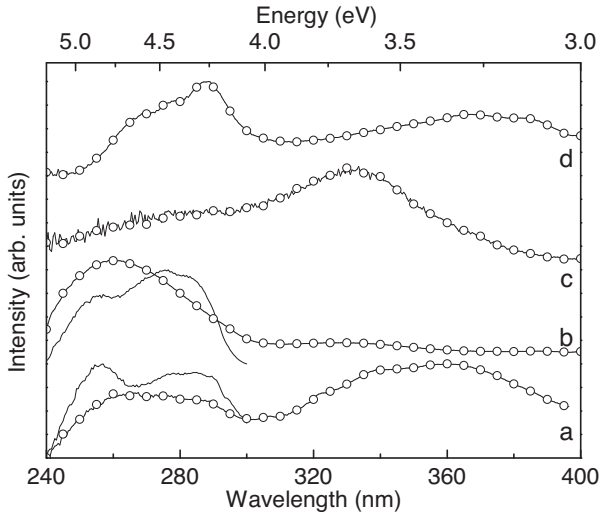

Figure 6. Room temperature excitation spectra of the ZrO_2 nanoparticles (a) synthesized in benzyl alcohol at 250 °C, (c) in biphenyl methanol, (d) modified with undecanoic acid. (b) Excitation spectra acquired at 12 K for the sample synthesized in benzyl alcohol at 250 °C. Monitored at 320 nm (solid line), 440 nm (lines with circles).

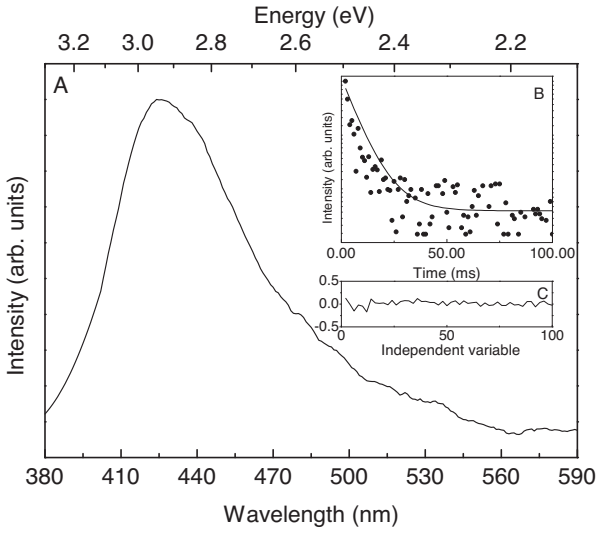

Figure 7. (A) Room temperature time-resolved emission spectrum (SD = 0.05×10^{-3} s, integration window = 20.00×10^{-3} s) of zirconia nanoparticles synthesized in benzyl alcohol at 300 °C excited at 350 nm. (B) Emission decay curve monitored at 440 nm. The solid line represents the data best fit ($\chi_{red}^2 = 2.7 \times 10^{-3}$), using a single exponential function. (C) The respective regular residual plot is also shown for a better judgment of the fit quality.

defects and/or the activation of Ti^{IV} impurities present in ppm concentrations in the zirconia lattice.[35,36]

The emission features acquired at room temperature resemble those measured at 12 K showing a red-shift of the low-wavelength emission component from ca. 320 to 370 nm and a shoulder band located around 420 nm (Figure 5a). The excitation spectra acquired at 300 K is also similar to that measured at 12 K revealing, however, a variation in the relative intensity of the UV components at *ca.* 260 and 290 nm and an increase in the relative intensity of the high-wavelength band (Figure 6a).

Varying the synthesis temperature from 300 °C to 250 °C does not induce major changes in the photoluminescence spectra (Figure S1 in the Supporting Information).

The emission features were quantified trough the measurement of the absolute emission quantum yield at different excitation wavelengths as a function of the synthesis temperature. For the sample synthesized at 250 °C the quantum yield values are 0.04 ± 0.01 in the excitation wavelength interval between 290 and 365 nm. For the sample prepared at 300 °C the same values were measured within the experimental error, reinforcing that the synthesis temperature value in the interval 250–300 °C does not induce major changes in the photoluminescence features, as already pointed by the emission and excitation spectra discussed above. These quantum yield values are more than one order of magnitude higher when compared to the value obtained in zirconia nanoparticles of similar size.[34] This is attributed to the contribution of the benzoate species to the overall emission features.

Time-resolved spectroscopy provides further arguments indicating that the emission features result from the overlap of two distinct contributions, that is, being related to the emission of the benzoate species and the ZrO_2 nanoparticles. The benzoate-related emission was selectively studied by time resolved spectroscopy excited at 350 nm. **Figure 7** illustrates the room temperature time-resolved emission spectrum acquired from zirconia nanoparticles synthesized in benzyl alcohol at 300 °C using a starting delay (SD) value of 0.05×10^{-3} s, revealing the presence of a long lived emission band centered at *ca.* 440 nm, which, apart from a decrease in the FWHM around 20%, overlaps the emission spectra acquired in steady state regime (Figure 5, Figure S2 of Supporting Information). The emission decay curve monitored at the maximum intensity peak position (440 nm) is well fitted with single exponential function (Figure 7B, Figure S3 of Supporting Information) yielding to lifetime value of 9.2 ± 0.8×10^{-3} s. Such a long-lived emission is completely in agreement with the triplet nature assignment.[37,38]

In order to study the time scale behind the emission features of the high-energy ZrO_2-related emission, time resolved spectroscopy was performed using an excitation wavelength of 330 nm (**Figure 8**).

The time-resolved emission features in the 10^{-9} s time scale reveal the presence of a broad band peaking at 410 nm (3.00 eV), which is red-shifted (0.45 eV) relatively to the corresponding steady-state emission spectra (Figure 8), providing strong evidence of the fact that this emission component is governed by a recombination mechanism typical of donor-acceptor (D–A) pairs, mediated by some defect centers.[39,40] The emission decay curves were monitored along the emission band between 380 and 500 nm, revealing a single exponential behavior for time values above 18.40 ns (Figure 8B and Figure S3 in the Supporting Information) suggesting the presence of a single emission component. The single exponential behavior is a direct evidence that the emission mechanisms in that time range are dominated by the radiative decay, pointing out a low distribution of emitting centers.[41,42] The lifetime values increase (25%) from $3.18 \pm 0.04 \times 10^{-9}$ s to $3.98 \pm 0.08 \times 10^{-9}$ s, as the monitoring wavelength increases from 390 to 500 nm,

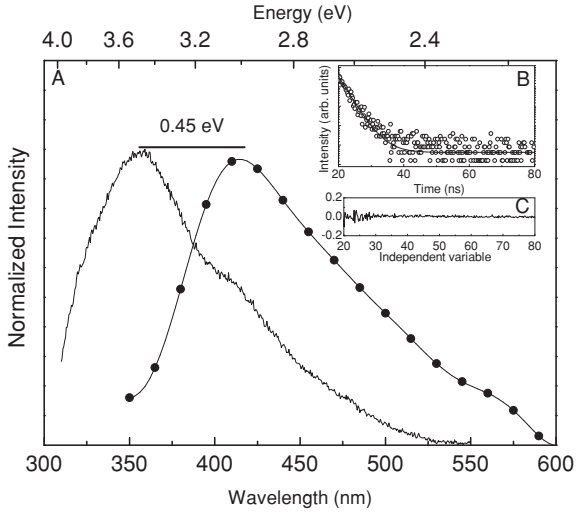

Figure 8. (A) Emission spectra of zirconia nanoparticles synthesized in benzyl alcohol at 300 °C recorded at 300 K in steady state (solid line) and time-resolved (line with circles, SD = 22.0 ns) excited at 330 nm. (B) Emission decay curve monitored at 413 nm. The solid line represents the data best fit ($\chi_{red}^2 = 1.3 \times 10^{-4}$), using a single exponential function $I(t) = I_0 \times exp(-(t-t_0)/\tau)$, where I_0 is the intensity at $t = t_0 = 18.40$ ns. (C) The respective regular residual plot is also shown for a better judgment of the fit quality.

corroborating the presence of *D-A* related emission, as distant pairs have a smaller recombination probability[[39,40]] A similar behavior was recently reported for silica based nanoparticles and was attributed to an exceptionally broad inhomogeneous distribution of the emitting centers.[43,44]

Further arguments supporting the cooperative effect of ZrO_2-related defects and of the organic ligands for the overall emission features of the benzoate capped ZrO_2 nanoparticles are obtained from the study of the optical properties of two similar samples, that is, the 3.2 nm zirconia nanoparticles stabilized by a layer of biphenolate species synthesized using biphenyl-4-methanol instead of benzyl alcohol as solvent and, the ZrO_2 synthesized in benzyl alcohol and further modified by ligand exchange with undecanoic acid. The emission spectra of these two samples are shown in Figure 5c and d. Under excitation wavelengths in the range 350–400 nm the emission features of the biphenolate-stabilized nanoparticles display a large single band typically ascribed to the biphenyl triplet exited states.[29i] Decreasing the excitation wavelength, the maximum intensity peak position deviates towards the blue, indicating the presence of the ZrO_2-related low-wavelength component. The excitation spectra monitored at the biphenyl triplet exited states (440 nm) shows a broad (FWHM ca. 60 nm) band peaking at 330 nm attributed to the excitation of the phenyl rings of the biphenolate species.[29i] This peak is blue-shifted when compared to the one in the spectra of the benzoate-stabilized nanoparticles (cf. Figure 5a), pointing out that the high-wavelength component present in the emission and excitation spectra of the ZrO_2 nanoparticles synthesized in benzyl alcohol is related to the organic ligand. Further support to such observation can be found in the analysis of the photoluminescence features of the nanoparticles in which the benzoate species were replaced by undecanoic acid. The sample excited between 350 and 400 nm also shows emission related to the benzoate (Figure 5d), indicating a partial replacement of the benzoate species, in agreement with the FT-IR study. Decreasing the excitation wavelength (280–300 nm) the emission spectra reveals also the presence of the ZrO_2-related emission with higher relative intensity. Such increase in the relative intensity for the undecanoic acid-stabilized nanoparticles is due to the decrease in the number of benzoate species, which favors the ZrO_2-related emission, further supporting that the high- and low-wavelength side of the emission spectra can be attributed to the presence of the organic species and ZrO_2-related defects, respectively. The excitation spectrum monitored at the emission maximum of the benzoate species (440 nm) shows similar features compared to the benzoate-stabilized sample (Figure 6a). However, a decrease in the relative intensity of the long-wavelength band due to the partial replacement of the benzoate group by the undecanoic acid can be noticed.

The incorporation of the Eu^{3+} ions in the nanoparticles confers additional photoluminescence features due to the presence of the emission arising from the intra-$4f^6$ transitions (**Figure 9**A).[9]

The emission features of the Eu^{3+}-doped nanoparticles consist of a broad band ascribed to the presence of ZrO_2-related

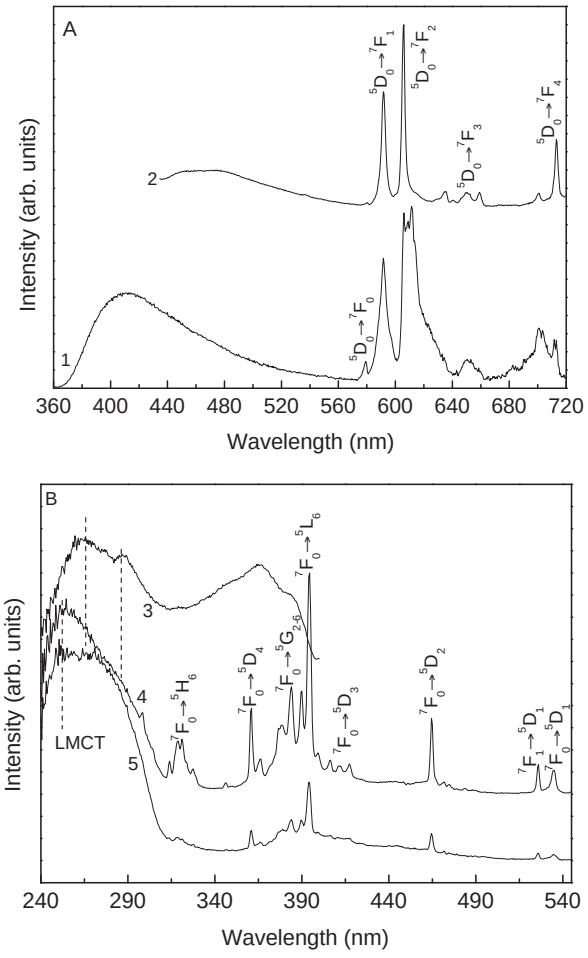

Figure 9. Room temperature (A) emission and (B) excitation spectra of Eu^{3+}-doped nanoparticles excited at (1) 285 nm and (2) 393 nm and monitored at (3) 445 nm, (4) 605 nm and (5) 611 nm.

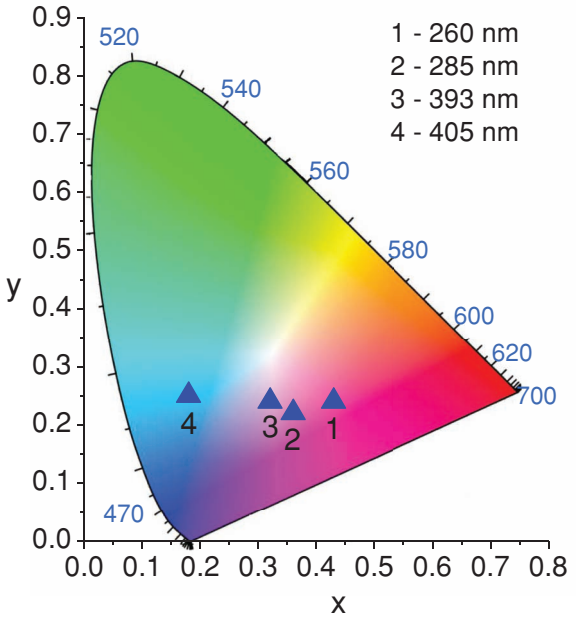

Figure 10. CIE chromaticity diagram showing the (x,y) emission color coordinates of the Eu^{3+}-doped nanoparticles excited at between 260 and 405 nm.

defects and the excited states of the benzoate species (Figure 5) and of the Eu^{3+} intra-$4f^6$ $^5D_0 \rightarrow {}^7F_{0-4}$ transitions. The contribution of the intra-$4f^6$ transitions and of the ZrO_2- and benzoate-related components enables the emission color tuning along the (Commission Internationale d'Eclairage (CIE) chromaticity diagram) by selecting the excitation wavelength (**Figure 10**). Increasing the excitation wavelength from 260 to 405 nm, the (x,y) color coordinates change from the purplish-pink region (0.43,0.24) to the greenish-blue area (0.18,0.25), respectively.

Focusing on the Eu^{3+} intra-$4f^6$ emission, it is observed that the energy, FWHM and number of Stark components strongly depend on the excitation wavelength (most evident for the $^5D_0 \rightarrow {}^7F_2$ transition), pointing out the presence of, at least, two distinct Eu^{3+}-local environments. In order to characterize the selective excitation paths for each Eu^{3+}-local environment, the excitation spectra were monitored into two distinct $^5D_0 \rightarrow {}^7F_2$ Stark components around 605 and 611 nm (Figure 9B). All the spectra reveal a component at *ca.* 250 nm attributed to a ligand-to-metal charge transfer (LMCT) band[29i,45] and the presence of two other components at *ca.* 260 and 290 nm also present in the excitation spectra of the pure nanoparticles (Figure 6). These two latter components (*ca.* 260 and 290 nm) are also observed in the excitation spectra monitored within the broad band emission (curve 3, Figure 9B) ascribed to the benzoate- and ZrO_2-related defects excited states. These broad band components are overlapped by a series of intra-$4f^6$ lines ascribed to transitions between the $^7F_{0,1}$ levels and the $^5H_6$, $^5D_{4-1}$, $^5G_{2-6}$, $^5L_6$ excited states. The dependence of the relative intensity between the intra-$4f^6$ transitions and the broad band components on the monitoring wavelength is another indication of the presence of, at least, two distinct Eu^{3+}-local coordination sites. The excitation spectrum monitored at 605 nm shows a high relative intensity of the Eu^{3+} transitions, pointing out that one local environment is mainly excited via direct intra-$4f^6$ excitation (labeled as Eu-Site1) rather than excitation via the LMCT band and the benzoate excited states, contrarily to that found in the excitation spectrum monitored at 611 nm, in which the main excitation path is through the LMCT and benzoate levels (labeled as Eu-Site2). It should be noted, that in both cases, there is an effective energy transfer from the nanoparticles host-to-Eu^{3+} ions which is active at room temperature.

In order to further detail the Eu^{3+} local coordination, the intra-$4f^6$ lines were measured at 10 K (Figure S4 of the Supporting Information). These spectra resemble those acquired at room-temperature revealing the presence of, at least, two Eu^{3+}-local coordination sites. The emission arising from Eu-Site1 (mainly excited via intra-$4f^6$ lines) is characterized by the high-intensity of the $^5D_0 \rightarrow {}^7F_2$ transition peaking at 605 nm, whereas the emission spectra arising from Eu-Site2 shows an increase in the relative intensity of the $^5D_0 \rightarrow {}^7F_{0,1}$ transitions and a broadening of the $^5D_0 \rightarrow {}^7F_2$ transition. Therefore, the Eu-Site1 $^5D_0$ emission decay curves (10 K and 300 K) were monitored at 605 nm and for Eu-Site2 the emission decay curves were monitored within the $^5D_0 \rightarrow {}^7F_0$ transition around 579.5 nm (Figure S5 of the Supporting Information). All the emission decay curves are well modeled by a single exponential function yielding to lifetime values for Eu-Site1 of 2.928 ± 0.027 ms and 2.841 ± 0.018 ms and for Eu-Site2 of 0.692 ± 0.057 ms and 0.666 ± 0.005 ms at 10 K and 300 K, respectively. The distinct path observed for the excitation of the two Eu-sites and the rather different $^5D_0$ lifetime values suggest that the Eu^{3+} ions in Eu-Site1 and Eu-Site2 are the Eu^{3+} ions located in the interior and on the surface of the nanoparticles, respectively. That is, Eu-Site1 is only coordinated via Eu-O-Zr bonds while Eu-Site2 is coordinatated via Eu-O-Zr and via Eu-O-C to the benzoates moieties.

Finally, **Figure 11** summarizes the possible electron transition pathways evidenced and discussed in this work for the

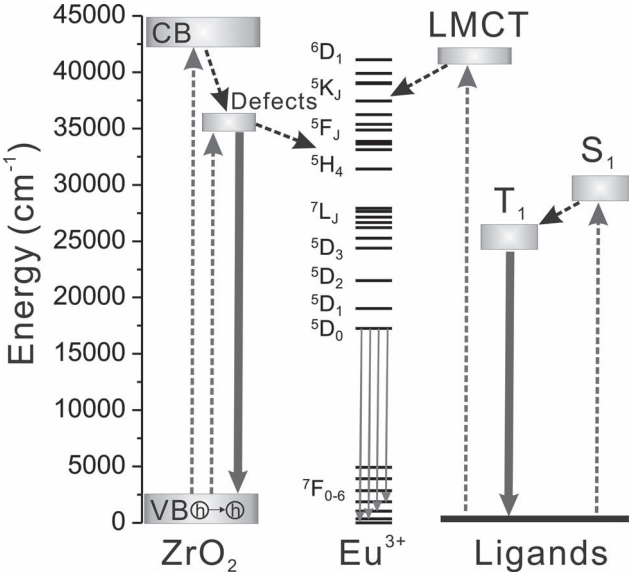

Figure 11. Energy levels and possible relaxation pathways in the Eu^{3+}-doped ZrO_2 nanoparticles. Full lines represent the radiative transitions and the dotted lines the non-radiative ones.

Eu^{3+}-doped zirconia nanoparticles. The energy level diagram includes the ZrO_2-related defect states, energy states of the ligands and the intra-$4f^6$ levels of Eu^{3+} ions. The observed radiative transitions are depicted by full lines.

3. Conclusion

Zirconia and Eu-stabilized zirconia nanoparticles were synthesized under nonaqueous conditions using different organic solvents (benzyl alcohol and biphenyl-4-methanol) and reaction temperatures (250 and 300 °C). The results demonstrate that the nature of the aromatic alcohol as well as the synthesis temperature only slightly influences the size, morphology and crystallinity of the nanoparticles. All the syntheses lead to highly crystalline and uniform 3–4 nm particles. However, differences were found on the amount and the nature of the organic species stabilizing the nanoparticles. Benzoate-, biphenolate-, and undecanoic acid-stabilized nanoparticles could be obtained in only one reaction step or by post-synthesis ligand exchange.

Under UV excitation, broad emission bands spanning from UV to the visible regions were observed. They depend on the excitation wavelength and the nature of the capping ligands. These emission bands were attributed to a cooperative effect between the capping ligands and defects associated to the ZrO_2 nanoparticles. When doped with Eu^{3+} ions the emission features due to the intra-$4f^6$ $^5D_0 \rightarrow {}^7F_{0-4}$ transitions are superimposed to the bands observed in undoped ZrO_2-capped nanoparticles. This allowed to tune the emission color by simply changing the excitation wavelength and to assess the local environment of the emitting centers.

4. Experimental Section

Synthesis: Zirconium(IV) isopropoxide isopropanol complex (99.9%), europium(III) acetate hydrate (99.9%), and benzyl alcohol (99%) were purchased from Aldrich. Biphenyl-4-methanol (98%) was purchased from Alfa Aesar. All the reagents and solvent were used directly without further purification. The ZrO_2 nanoparticles were synthesized by a procedure similar to the one reported previously.[9,13,29e,f,j] The syntheses were carried out in a glove box (O_2 and H_2O <1 ppm). For the synthesis of pure zirconium oxide nanoparticles zirconium isopropoxide isopropanol complex (500 mg) was added to benzyl alcohol (15 mL) in a glass vial. The glass vial was inserted into a steel autoclave, and sealed carefully. The autoclave was removed from the glove box and heated in the oven at 250 °C or 300 °C for 36h. In the case of the Eu^{3+} ions doped nanoparticles europium(III) acetate hydrate (9 mg) was added to zirconium isopropoxide isopropanol complex (490 mg) and the reaction was carried out at 300 °C for 36h. In order to investigate the influence of the organic solvent on the nanoparticles, benzyl alcohol was replaced by biphenyl-4-methanol. Zirconium(IV) isopropoxide isopropanol complex (200 mg) was added to biphenyl-4-methanol (10 g) and solvothermally treated at 300 °C for 36h. The resulting precipitates were centrifuged and washed thoroughly with ethanol and acetone, and subsequently dried in air at 60 °C. All as-synthesized samples are obtained as white powders.

For the post-synthesis ligand exchange, ZrO_2 nanoparticles (25 mg) synthesized at 300 °C were redispersed in ethanol (7 mL) and exposed to ultrasonication for 1 hour. Afterward, a solution of undecanoic acid (35 mg) in ethanol (8 mL) was added under vigorous stirring. The resulting mixture was left under stirring at room temperature for 24 h. A slightly opalescent dispersion was obtained. The functionalized nanoparticles were centrifuged, washed thoroughly with acetone and subsequently dried in air at 60 °C.

Characterization: The X-ray powder diffraction (XRD) patterns of all samples were measured in reflection mode (Cu Kα X-ray at 45 kV and 40 mA) on a X'Pert MPD Philips diffractometer. The patterns were measured in the 2θ range from 3.00 to 70.00° with a step of 0.02°. For transmission electron microscopy (TEM) measurements, one or two drops of the solution of the nanoparticles in ethanol were deposited on a copper grid coated with a lacey amorphous carbon film. A Jeol 2200FS microscope equipped with an in column energy filter and a field emission gun operated at 200 kV, or a Hitachi H-9000 operated at 300 kV were used. Fourier transform infrared spectra (FT-IR) measurements were carried out on a Brucker Optics Tensor 27 spectrometer in the range of 4000–350 cm^{-1} in transmission mode. The pellets were prepared by adding nanoparticles powder (1–2 mg) to KBr (100 mg). The mixture was carefully homogenized and compressed with an uniaxial pressure of 9 MPa. Carbon, hydrogen, and nitrogen elemental analyses (CHN) were performed using a CHNS-932 elemental analyzer with standard combustion conditions and handling of the samples in air. The organic ligands attached to the surface of the particles upon drying were also analyzed by solid state nuclear magnetic resonance (SS-NMR) on a BRUKER AVANCE 400 spectrometer equipped with a 2.5 mm CP/MAS probe.

Optical studies: The photoluminescence spectra were recorded at room temperature and at 12K with a modular double grating excitation spectrofluorimeter with a TRIAX 320 emission monochromator (Fluorolog-3, Horiba Scientific) coupled to a R928 Hamamatsu photomultiplier, using a front face acquisition mode. The excitation source was a 450 W Xe arc lamp. The emission spectra were corrected for detection and optical spectral response of the spectrofluorimeter and the excitation spectra were corrected for the spectral distribution of the lamp intensity using a photodiode reference detector. The time resolved spectroscopy (emission spectra and emission decay curves) were measured at 12 K with the setup described for the luminescence spectra using a pulsed Xe–Hg lamp (6 µs pulse at half width and 20–30 µs tail). The room temperature time-resolved spectroscopy data were recorded on a Fluorolog TCSPC spectrofluorimeter (Horiba Scientific) coupled to a TBX-04 photomultiplier tube module (950 V), 200 ns time-to-amplitude converter and 70 ns delay. The excitation source was a Horiba-Jobin-Yvon pulsed diode (NanoLED-330, peak at 330 nm, 1.2 ns pulse duration, 1 MHz repetition rate and 150 ns synchronization delay).

The absolute emission quantum yields were measured at room temperature using a quantum yield measurement system C9920-02 from Hamamatsu with a 150 W Xenon lamp coupled to a monochromator for wavelength discrimination, an integrating sphere as sample chamber and a multi-channel analyzer for signal detection. Three measurements were made for each sample so that the average value is reported. The method is accurate to within 10%.

Supporting Information

Supporting Information is available from the Wiley Online Library or from the author.

Acknowledgements

This work was partially supported by the WCU (World Class University) program through the National Research Foundation (NRF) of Korea funded by the Ministry of Education, Science and Technology (R31-10013) and by FCT PEst-C/CTM/LA0011/2011, SFRH/BPD/71671/2010 and SFRH/BD/45177/2008. We are grateful to Marc-Georg Willinger from the Fritz Haber Institute of the Max Planck Society and, Marta C. Ferro and Gianvito Caputo from the University of Aveiro for TEM measurements. Guylhaine Clavel from the University of Montpellier II

and Markus Niederberger from the ETH Zurich are acknowledged for critical reading of the manuscript and fruitful discussions.

Received: March 19, 2012
Published online: June 19, 2012

[1] E. D. Wachsman, K. T. Lee, *Science* **2011**, *334*, 935.
[2] M. Tsuchiya, B. K. Lai, S. Ramanathan, *Nat. Nanotechnol.* **2011**, *6*, 282.
[3] M. Roeb, H. M. Steinhagen, *Science* **2010**, *329*, 773.
[4] A. Adamski, P. Zapala, L. Chmielarz, J. A. J. Rodriguez, G. Djega-Mariadassou, Z. Sojka, *Catal. Today* **2011**, *176*,.
[5] S. Souentie, L. Lizarraga, A. Kambolis, M. Alves-Fortunato, J. L. Valverde, P. Vernoux, *J. Catal.* **2011**, *283*, 124.
[6] D. He, Y. Ding, H. Luo, C. J. Li, *J. Mol. Cata.* **2004**, *208*, 267.
[7] G. D. Liu, Y. H. Lin, *Ana. Chem* **2005**, *77*, 5894.
[8] H. Tsuchiya, J. M. Macak, L. Taveira, P. Schmuki, *Chem. Phys. Lett* **2005**, *410*, 188.
[9] T. Ninjbadgar, G. Garnweitner, A. Borger, L. M. Goldenberg, O. V. Sakhno, J. Stumpe, *Adv. Funct. Mater.* **2009**, *19*, 1819.
[10] N. Zhao, D. Pan, W. Nie, X. Ji, *J. Am. Chem. Soc.* **2006**, *128*, 10118.
[11] J. Robertson, *J. Vac. Sci. Technol. B* **2000**, *18*, 1785.
[12] A. Emeline, G. V. Kataeva, A. S. Litke, A. V. Rudakova, V. K. Ryabchuk, N. Serpone, *Langmuir* **1998**, *14*, 5011.
[13] G. Garnweitner, L. M. Goldenberg, O. V. Sakhno, M. Antonietti, M. Niederberger, J. Stumpe, *Small* **2007**, *3*, 1626.
[14] R. Landsiedel, L. Ma-Hock, A. Kroll, D. Hahn, J. Schnekenburger, K. Wiench, W. Wohlleben, *Adv. Mater.* **2010**, *22*, 2601.
[15] C. M. Zhang, C. X. Li, J. Yang, Z. Y. Cheng, Z. Y. Hou, Y. Fan, J. Lin, *Langmuir* **2009**, *25*, 7078.
[16] J. H. Liang, Z. X. Deng, X. Jiang, F. L. Li, Y. D. Li, *Inorg. Chem.* **2002**, *41*, 3602.
[17] Y. Cong, B. Li, S. M. Yue, D. Fan, *J. Phys. Chem. C* **2009**, *113*, 13974.
[18] Z. Wang, B. Yang, Z. Fu, W. Dong, Y. Yang, W. Liu, *Appl. Phys. A* **2005**, *81*, 691.
[19] K. Smits, L. Grigorjeva, W. Lojkowski, J. D. Fidelus, *Phys. Stat. Sol. C* **2007**, *4*, 770.
[20] L. L. Chen, T. Mashimo, E. Omurzak, H. Okudera, C. Iwamoto, A. Yoshiasa, *J. Phys. Chem. C* **2011**, *115*, 9370.
[21] Q. L. Dai, M. E. Foley, C. J. Breshike, A. Lita, G. F. Strouse, *J. Am. Chem. Soc.* **2011**, *133*, 15475.
[22] E. F. Schebert, J. K. Kim, *Science* **2005**, *308*, 1274.
[23] T. Narukawa, M. Ichikawa, D. Sanga, M. Sano, T. Mukai, *J. Phys. D: Appl. Phys.* **2010**, *43*, 354002-1–354002-6.
[24] H. R. Chen, J. L. Shi, Y. Yang, Y. S. Li, D.-S. Yan, C. S. Shi, *Appl. Phys. Lett.* **2002**, *81*, 2761.
[25] D. Vollath, D. V. Szabo, S. Schlabach, *J. Nanoparticle. Res.* **2004**, *6*, 181.
[26] Y. Haldprai, T. Q. Zong, J. J. Shim, *J. Appl. Polymer. Sci.* **2011**, *123*, 1176.
[27] C. Sanchez, B. Lebeau, F. Chaput, J. P. Boilot, *Adv. Mater.* **2003**, *15*, 1969.
[28] Z. G. Wang, X. T. Zu, S. Zhu, X. Xiang, L. M. Fang, L. M. Wang, *Phys. Lett. A* **2006**, *350*, 252.
[29] a) N. Pinna, M. Niederberger, *Angew. Chem. Int. Ed.* **2008**, *47*, 5292; b) M. Niederberger, *Acc. Chem. Res.* **2007**, *40*, 793; c) N. Pinna, G. Garnweitner, P. Beato, M. Niederberger, M. Antonietti, *Small* **2005**, *1*, 112; d) M. Karmaoui, R. A. S. Ferreira, A. T. Mane, L. D. Carlos, N. Pinna, *Chem. Mater.* **2006**, *18*, 4493; e) G. Clavel, M.-G. Willinger, D. Zitoun, N. Pinna, *Adv. Funct. Mater.* **2007**, *17*, 3159; f) N. Pinna, *J. Mater. Chem.* **2007**, *17*, 2769; g) A. Pucci, G. Clavel, M.-G. Willinger, D. Zitoun, N. Pinna, *J. Phys. Chem. C* **2009**, *113*, 12048; h) R. A. S. Ferreira, M. Karmaoui, S. S. Nobre, L. D. Carlos, N. Pinna, *Chem. Phys. Chem.* **2006**, *7*, 2215; i) M. Karmaoui, L. Mafra, R. A. S. Ferreira, J. Rocha, L. D. Carlos, N. Pinna, *J. Phys. Chem. C* **2007**, *111*, 2539; j) A. Pucci, M.-G. Willinger, F. Liu, X. Zeng, V. Rebuttini, G. Clavel, X. Bai, G. Ungar, N. Pinna, *ACS Nano* **2012**, *6*, 4382.
[30] K. D. Dobson, A. J. Mcquillan, *Spectrochim. Acta A* **2000**, *56*, 557.
[31] X. H. Guan, G. H. Chen, C. Shang, *J. Environ Sci.* **2007**, *19*, 438.
[32] W. F. Dong, R. Wang, G. Mao, H. Mohwald, *Soft Matter* **2006**, *2*, 686.
[33] S. Pawsey, K. Yach, J. Halla, L. Reven *Langmuir* **2000**, *16*, 3294.
[34] J. Joo, T. Yu, Y. W. Kim, H. M. Park, F. X. Wu, J. Z. Zhang, T. Hyeon, *J. Am. Chem. Soc.* **2003**, *125*, 6553.
[35] F. Gallino, C. D. Valentin, G. Pacchioni, *Phys. Chem. Chem. Phys.* **2011**, *13*, 17667.
[36] A. S. Foster, V. B. Sulimov, F. Lopez Gejo, A. L. Shluger, R. M. Nieminen, *Phys. Rev. B* **2001**, *64*, 224108.
[37] B. Hiroaki, K. Michio, *J. Mol. Spectrum.* **1972**, *41*, 302.
[38] D. J. Morantz, A. J. C. Wright, *J. Chem. Phys.* **1971**, *54*, 692.
[39] N. Chestnoy, T. D. Harris, R. Hull, L. E. Brus, *J. Phys. Chem.* **1986**, *90*, 3393.
[40] Y. Zhong, K. S. Wong, W. Zhang, D. C. Look, *Appl. Phys. Lett.* **2006**, *89*, 022108.
[41] C. Delerue, G. Allan, C. Reynaud, O. Guillois, G. Ledoux, F. Huisken, *Phys. Rev. B* **2006**, *73*, 235318.
[42] S. F. Wuister, C. de Mello Donegá, A. Meijerink, *J. Chem. Phys.* **2004**, *121*, 4310.
[43] C. D. S. Brites, V. T. Freitas, R. A. S. Ferreira, A. Millán, F. Palacio, L. D. Carlos, *Langmuir* **2012**, *28*, 8190.
[44] L. Vaccaro, G. Vaccaro, S. Agnello, G. Buscarino, M. Cannas, *Solid State. Commun.* **2010**, *150*, 2278.
[45] G. Blasse, B. C. Grabmaier, *Luminescent materials*, Springer, Berlin, Germany **1994**.